

Altermagnetic type-II Multiferroics with Néel-order-locked Electric Polarization

Wen-Ti Guo^{1,*}, Junqi Xu^{1,*}, Huaiqiang Wang^{2,†} and Haijun Zhang^{1,3,4‡}

¹ National Laboratory of Solid State Microstructures,

School of Physics, Nanjing University, Nanjing 210093, China

² Center for Quantum Transport and Thermal Energy Science,

School of Physics and Technology, Nanjing Normal University, Nanjing 210023, China

³ Collaborative Innovation Center of Advanced Microstructures,

Nanjing University, Nanjing 210093, China and

⁴ Jiangsu Physical Science Research Center, Nanjing 210093, China

Altermagnetism, an emergent magnetic phase featuring compensated collinear magnetic moments and momentum-dependent spin splittings, has recently garnered widespread interest. A pivotal issue concerns whether the unconventional spin structures can generate spontaneous electric polarization in altermagnets, thereby achieving type-II multiferroicity. Here, with the combination of symmetry analysis and microscopic theory, we explicitly demonstrate the generation of electric polarization by altermagnetic Néel order, and establish a microscopic mechanism of Néel-order-locked electric polarization in altermagnetic multiferroics. We further reveal these pronounced magnetoelectric coupling behaviors and classify them into eight distinct categories for two-dimensional altermagnets governed by layer group symmetries. Then we take monolayer MgFe_2N_2 as a prototypical example of altermagnetic multiferroics by first-principles calculations. We also propose to identify the Néel order orientation and accompanying electric polarization in altermagnetic multiferroics by magneto-optical microscopy. Bridging type-II multiferroics and altermagnets, our work could pave the way for altermagnetic multifunctional spintronics.

Introduction. Altermagnetism, an emerging magnetic phase characterized by compensated collinear magnetic moments and momentum-dependent spin splittings, represents a new class of magnetic materials beyond traditional ferromagnets and antiferromagnets [1–32]. Uniquely bridging ferromagnetic and antiferromagnetic characteristics, altermagnets could exhibit time-reversal-breaking magneto responses and simultaneously display negligible stray fields and high-frequency spin dynamics, making them promising candidates in ultra-fast spintronic devices [8, 33–38]. While recent experimental advances employing techniques such as angle-resolved photoemission spectroscopy [7, 9, 10], magneto-optical microscopy [39–41], and anomalous Hall measurements [42, 43], have validated the unconventional electronic and magnetic signatures in altermagnets [43–45], magnetoelectric (ME) coupling effects of altermagnets remain elusive and have become a prominent research focus [46–52]. Critically, the interplay between unconventional magnetic order and emergent electric polarization remains unexplored, hindering the design of altermagnetic memory and logic devices.

Multiferroicity, characterized by the coexistence of ferroelectricity and magnetism in a single-phase material, provides a unique perspective to investigate ME coupling mechanisms in magnetic systems. Multiferroic materials are broadly classified into type-I and type-II, with the latter demonstrating significantly stronger intrinsic ME coupling due to their magnetic-order-driven ferroelectricity. However, most experimentally reported type-II multiferroic materials have noncollinear magnetic order, whose complex response to external fields may significantly hinder the manipulation of ME effects [53–55]. Therefore, achieving type-II multiferroicity in materials

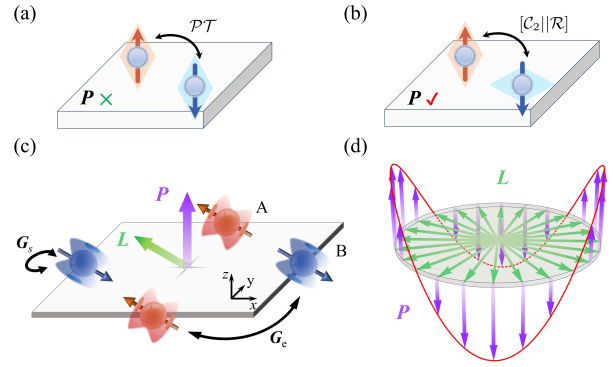


FIG. 1. Schematic of altermagnetic-induced multiferroics. Illustration of electric polarization in (a) conventional \mathcal{PT} -symmetric antiferromagnets and (b) altermagnets. In (a), the two opposite magnetic sublattices are related via \mathcal{PT} symmetry, leading to compensated electric dipole moments and vanishing spontaneous electric polarization \mathbf{P} . Whereas in (b) the two sublattices are not connected by inversion, and thus finite \mathbf{P} is generally permissible. (c) Illustration of the locking behavior between \mathbf{P} and Néel order \mathbf{L} in altermagnets, which results from constraints imposed by \mathcal{G}_s and \mathcal{G}_e symmetries connecting the same and different sublattices, respectively. (d) Typical locking behavior between out-of-plane \mathbf{P} and in-plane \mathbf{L} orientation for category 5 altermagnetic multiferroics in our classification.

with collinear magnetic order is highly desirable. It has been proposed that collinear spin systems can develop ferroelectric polarization through p - d orbital hybridization, where crystal field effects break inversion symmetry at magnetic ion sites [56–58]. Given that altermagnets inherently combine collinear magnetic order with broken inversion symmetry, a pivotal question emerges: can their

unconventional spin structures induce spontaneous electric polarization, thus establishing a new paradigm for type-II multiferroicity?

In this letter, we employ symmetry analysis and microscopic theoretical modeling of electric dipole moments to definitively resolve the aforementioned issue by explicitly demonstrating the emergence of electric polarization induced by altermagnetic spin structures. Crucially, we establish a microscopic-level correlation between the electric polarization vector and the altermagnetic Néel order parameter, which unambiguously realizes type-II multiferroicity. Based on different locking behaviors between electric polarization and Néel order orientation, we further classify two-dimensional (2D) altermagnetic type-II multiferroics governed by layer group (LG) symmetries into eight distinct categories. In addition, our first-principles calculations of monolayer MgFe_2N_2 , a prototypical altermagnetic multiferroic material, robustly validate our theoretical framework. We also propose an experimental detection scheme via magneto-optical Faraday effect to determine the Néel order orientation and accompanying electric polarization in altermagnetic multiferroics. By integrating giant ME couplings of type-II multiferroics and unique advantages of altermagnets, our work provides a versatile platform for designing multifunctional devices.

Symmetry analysis and microscopic theory. The electric dipole moment is odd under spatial inversion operation \mathcal{P} while even under time-reversal operation \mathcal{T} . Consequently, in conventional \mathcal{PT} -symmetric antiferromagnets where the two antiparallel magnetic sublattices are connected by inversion, as illustrated in Fig. 1(a), the electric dipole moments from the two sublattices strictly cancel out, leading to a vanishing total polarization \mathbf{P} . By contrast, since antiparallel magnetic sublattices in altermagnets are never connected by inversion, their electric dipole moments are no longer subject to the above symmetry constraint, and a nonzero macroscopic polarization is thus generally allowed to exist, as shown in Fig. 1(b).

We then start from the microscopic theory for electric dipole moments to derive the expression of electric polarization induced by altermagnetic order. We consider an altermagnet with two antiparallel magnetic sublattices labeled as A and B, respectively [see Fig. 1(c)], each hosting one magnetic ion per sublattice with spin $\mathbf{S}_{A(B)} = \pm\mathbf{S}$. The Néel vector is defined as $\mathbf{L} = \frac{1}{2}(\mathbf{S}_A - \mathbf{S}_B) = \mathbf{S}$. We further assume A and B sublattices occupy the same Wyckoff position of multiplicity two with the site symmetry group denoted as \mathcal{G}_s . In addition, for altermagnets, there always exists at least one space group symmetry operation connecting different sublattices, such as the fourfold rotation in Fig. 1(c), and we collect all such space group operations into a set denoted as \mathcal{G}_e . According to the microscopic mechanism [56–60], the local electric dipole moment from each magnetic sublattice can be represented as a linear combination of prod-

ucts of spins: $p_M^\alpha = [K_M]_{\beta\gamma}^\alpha S_M^\beta S_M^\gamma$, where p_M^α and S_M^α ($\alpha = x, y, z$, $M = A, B$) are the α -component of the electric dipole moment \mathbf{p}_M and spin \mathbf{S}_M in Cartesian coordinates, respectively, and the coefficient K_M is a real-symmetric third-rank polar tensor. Note that the existence of symmetry operations in $\mathcal{G}_s(\mathcal{G}_e)$ connecting the same (different) sublattices will impose constraints on the coefficient tensors [see Supplemental Material (SM) [61] for details], given by

$$[R_s]_{\alpha\beta} [K_M]_{\gamma\delta}^\beta = [R_s]_{\gamma\mu}^T [K_M]_{\mu\nu}^\alpha [R_s]_{\nu\delta}, \quad (1)$$

and

$$[R_e]_{\alpha\beta} [K_M]_{\gamma\delta}^\beta = [R_e]_{\gamma\mu}^T [K_{\bar{M}}]_{\mu\nu}^\alpha [R_e]_{\nu\delta}, \quad (2)$$

where R_s and R_e are the point group parts of the symmetry operations in \mathcal{G}_s and \mathcal{G}_e , respectively, and \bar{M} denotes different sublattices. These constraints will significantly reduce independent elements of the coefficient tensors K_A and K_B . In other words, the detailed form of the coefficient tensor is fully determined by the space group of the crystal and Wyckoff positions of the magnetic sublattices.

The total electric dipole moment per unit cell \mathbf{p}_{tot} can then be obtained by summing local electric dipole moments from the two sublattices, which can be expressed in the component form as

$$\mathbf{p}_{\text{tot}}^\alpha = [p_A]^\alpha + [p_B]^\alpha = [K_A + K_B]_{\beta\gamma}^\alpha L^\beta L^\gamma, \quad (3)$$

where L^β is the β -component of Néel vector \mathbf{L} . For an altermagnet containing N unit cells, the macroscopic electric polarization is simply given by $\mathbf{P} = N\mathbf{p}_{\text{tot}}$, indicating the direct correlation between polarization and Néel vector. Based on the microscopic theory, for conventional \mathcal{PT} antiferromagnets, according to Eq. (2), the inversion operation $\mathcal{P} = -\delta_{\alpha\beta}$ ($\alpha, \beta = x, y, z$) will lead to $K_A = -K_B$, thus resulting in $\mathbf{P} = 0$. By comparison, for altermagnets, we generically have $K_A \neq -K_B$ due to the lack of inversion, and thus a finite \mathbf{P} is permissible. Note that the above results from the microscopic theory are consistent with those from intuitive symmetry analysis.

Classification of 2D altermagnetic multiferroics. Atomically thin (quasi-2D) multiferroic materials demonstrate unique structural and functional advantages, including enhanced magnetoelectric coupling, ultralow energy consumption, and multifunctional device integration, making them ideal for cutting-edge applications such as next-generation nanoelectronics and flexible electronics [62–65]. Therefore, henceforth we will focus on the classification of type-II multiferroics in 2D altermagnets whose crystal symmetry is described by layer groups (LGs). A four-step classification scheme is implemented as follows. First, we systematically scrutinize all LGs, and identify the LGs containing Wyckoff positions of multiplicity two, which satisfy the symmetry requirement of altermagnets hosting two magnetic sublattices. Second, we extract the polar LGs belonging to type-I multiferroics (see the SM [61] for more details). Third, for the

TABLE I. List of layer groups (LGs) satisfying the symmetry requirements of both type-II multiferroics and 2D altermagnets with two magnetic sublattices. The sublattices occupy the same Wyckoff position with the multiplicity of two. Those LGs are classified into eight categories (Cat.), based on the dependence of polarization \mathbf{P} on the direction of Néel vector \mathbf{L} , with θ (ϕ) denoting the polar (azimuthal) angle of \mathbf{L} in spherical coordinates. The site symmetry (Site symm.) of each Wyckoff position is also given below. $A = \alpha \sin(2\theta)$, $B = \beta \sin^2 \theta$, $C = \gamma \sin(2\theta)$, $D = \delta \sin^2 \theta$, where $\alpha, \beta, \gamma, \delta$ are material-dependent constants, and θ and ϕ are the polar and azimuthal angles of \mathbf{L} , respectively.

Cat.	LG	Wyckoff	Site symm.	Polarization
1	19	2l,2k,2j,2i	..2	$\begin{bmatrix} A \sin \phi \\ C \cos \phi \\ B \sin(2\phi) \end{bmatrix}$
	20,21	2b,2a	..2	
2	50	2e,2d,2c	2..	$\begin{bmatrix} A \cos \phi + C \sin \phi \\ C \cos \phi - A \sin \phi \\ B \cos(2\phi) + D \sin(2\phi) \end{bmatrix}$
3	53	2e,2d(2c)	4..(222.)	$\begin{bmatrix} A \sin \phi \\ -A \cos \phi \\ 0 \end{bmatrix}$
	54	2b(2a)	4..(2.22)	
	76	2c	6..	
4	57	2e,2d(2c)	2.mm(222.)	$\begin{bmatrix} A \sin \phi \\ A \cos \phi \\ B \sin(2\phi) \end{bmatrix}$
	58	2b(2a)	2.mm(-4..)	
5	59	2e,2d,2c	2mm.	$\begin{bmatrix} A \cos \phi \\ -A \sin \phi \\ B \cos(2\phi) \end{bmatrix}$
	60	2b(2a)	2.22(-4..)	
6	67	2f,2e,2d	3..	$\begin{bmatrix} A \sin \phi + B \sin(2\phi) \\ -A \cos \phi + B \cos(2\phi) \\ 0 \end{bmatrix}$
7	68	2c,2b	3..	$\begin{bmatrix} A \sin \phi + B \cos(2\phi) \\ -A \cos \phi - B \sin(2\phi) \\ 0 \end{bmatrix}$
8	79	2b	-6..	$\begin{bmatrix} B \cos(2\phi) \\ -B \sin(2\phi) \\ 0 \end{bmatrix}$

remaining non-polar LGs, we exclude the LGs for which the site symmetry group of Wyckoff positions with multiplicity two contains inversion. Finally, we use Eqs. (1-2) to obtain the detailed form of electric polarizations \mathbf{P} as a function of Néel vector \mathbf{L} for each LG.

Based on different locking behaviors between polarization and the Néel vector orientation, we classify type-II multiferroics in 2D altermagnets into eight categories in terms of LGs, as presented in Table I, where θ and ϕ are the polar and azimuthal angles of \mathbf{L} in spherical coordinates. Notably, for all categories, each component of \mathbf{P} exhibits either π - or 2π -periodic behaviors with respect to azimuthal angle ϕ of \mathbf{L} . Specifically, we select category 5 as a representative case where \mathbf{L} lies in the x - y plane. In this case, the polarization is always out-of-plane with $P \propto \cos(2\phi)$, displaying a π -periodic dependence on the azimuthal angle of \mathbf{L} as illustrated in Fig. 1(d).

Candidate Material. To validate the preceding the-

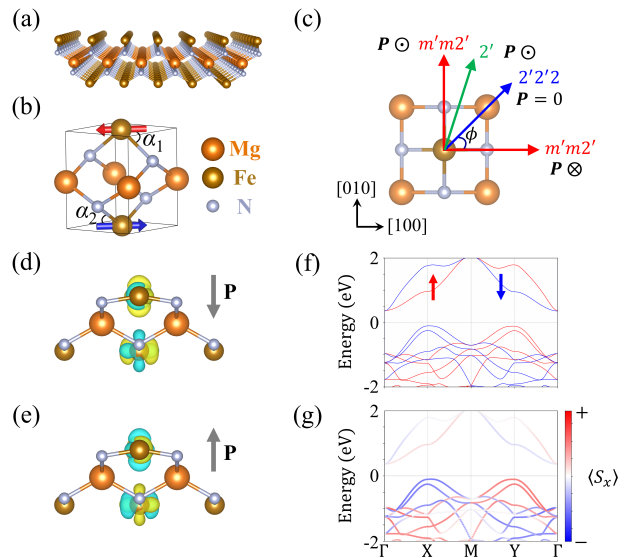


FIG. 2. Type-II multiferroicity in altermagnetic monolayer MgFe_2N_2 . (a-c) Crystal structure of monolayer MgFe_2N_2 in (a) front, (b) side, and (c) top views. The in-plane Néel order originates from Fe atoms. Magnetic point group symmetries and associated electric polarization for distinct Néel order orientations are summarized in (c). (d, e) The magnetic-order-induced charge density difference (compared to the paraelectric phase) around Fe atoms for the (d) inverse ferroelectric ($P_z < 0$) and (e) ferroelectric phases ($P_z > 0$) at $\phi = 0$ and $\phi = \pi/2$, respectively, where distinct charge transfer trends can be seen. (f, g) Spin-resolved band structures of monolayer MgFe_2N_2 (f) without and (g) with spin-orbit coupling, respectively, where the Néel vector is aligned along the $[100]$ -direction.

oretical framework, we propose monolayer MgFe_2N_2 as a representative material exhibiting altermagnetic type-II multiferroicity. The nonmagnetic state of monolayer MgFe_2N_2 [see Figs. 2(a-c)] crystallizes in LG No. 59, featuring nonpolar $\bar{4}2m$ point group symmetry. This indicates the absence of ferroelectricity in nonmagnetic monolayer MgFe_2N_2 . Our first-principles calculations and symmetry analysis identify altermagnetic ordering characterized by in-plane antiparallel alignment of magnetic moments from Fe atoms [see Fig. 2(b)] as the magnetic ground state of monolayer MgFe_2N_2 , which is energetically favorable over the in-plane parallel alignment by approximately $68 \text{ meV}/f.u.$ (see SM [61] for the total energy calculation). The calculated band structures without [Fig. 2(f)] and with spin-orbit coupling [Fig. 2(g)] demonstrate nearly identical energy spectra accompanied by pronounced momentum-dependent spin splittings (reaching 1 eV at some k points). This substantiates the altermagnetic state of monolayer MgFe_2N_2 , where spin-orbit coupling exerts negligible effects in energy spectra and magnetic order.

Monolayer MgFe_2N_2 is described by LG 59, thus belonging to category 5 in our classification of 2D altermagnetic type-II multiferroics. Since its ground state Néel order lies in the x - y plane, the electric polarization is ex-

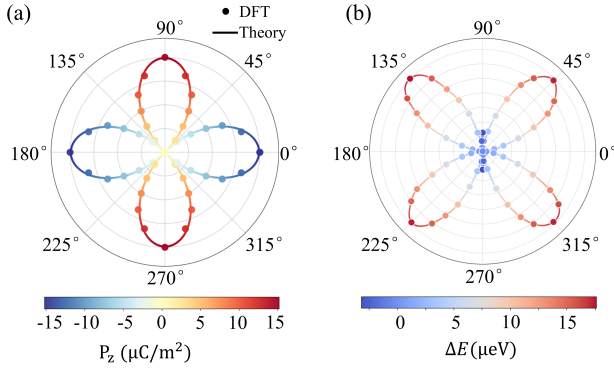


FIG. 3. First-principles calculations of (a) Néel-order-locked out-of-plane electric polarization and (b) total energy difference (compared to the minimum energy) as a function of in-plane Néel order orientations ($\phi = 0^\circ$ corresponds to the $[100]$ -direction) in altermagnetic monolayer MgFe_2N_2 .

pected to have only out-of-plane component P_z which is locked with the polar angle ϕ of the in-plane Néel order as $P_z \propto \cos(2\phi)$. This is confirmed by our first-principles calculations of the electric polarization as a function of the polar angle, as shown in Fig. 3(a), where P_z exhibits a π -periodic behavior of ϕ (the crystallographic $[100]$ -direction is set as $\phi = 0$). Specifically, P_z reaches maximal values of $\pm 15.2 \mu\text{C}/\text{m}^2$ at $\phi = n\pi/2$ ($n = 0, 1, 2, 3$) and vanishes at $\phi = (2n + 1)\pi/4$. Note that with varying ϕ from 0 to $\pi/2$ (or π to $3\pi/2$), there exists a sign reversal of the maximal P_z value from the inverse ferroelectric phase ($P_z < 0$) at $\phi = 0$ to the ferroelectric phase ($P_z > 0$) at $\phi = \pi/2$. Remarkably, this polarization switching process only requires overcoming a negligibly small energy barrier below $30 \mu\text{eV}$, as shown in Fig. 3(b), thus demonstrating the potential for efficient ME control of polarization through Néel order manipulation. In fact, the polarization switching process can also be understood by magnetic point group analysis. As illustrated in Fig. 2(c), during the in-plane rotation of \mathbf{L} , the system transitions sequentially from the polar magnetic point group $m'm'2'$ at $\phi = 0$ to the nonpolar phase $2'2'2$ at $\phi = \pi/4$ ($P_z = 0$) via an intermediate polar phase $2'$ at other angles, eventually recovering $m'm'2'$ symmetry at $\phi = \pi/2$.

Further, based on the p - d hybridization theory [56, 58–60, 66, 67] for type-II multiferroics, we give a microscopic explanation for altermagnetic multiferroicity in monolayer MgFe_2N_2 as follows. As the local crystal field of MgFe_2N_2 breaks inversion symmetry [see Fig. 2(b)], the even-parity d orbitals of Fe ions mix up with the odd-parity p orbitals of the ligand N ions, inducing the non-zero electric dipole $\mathbf{p} \propto \sum_i (\mathbf{S} \cdot \hat{\mathbf{e}}_i)^2 \hat{\mathbf{e}}_i$, where \mathbf{S} represents the spin of Fe ion, while $\hat{\mathbf{e}}_i$ denotes the unit vector along the i -th Fe-N bond. As a result, the polarization in MgFe_2N_2 directly originates from its magnetic structures, demonstrating robust intrinsic ME coupling. For in-plane spins $\mathbf{S} = (S_x, S_y, 0) \propto (\cos \phi, \sin \phi, 0)$, the

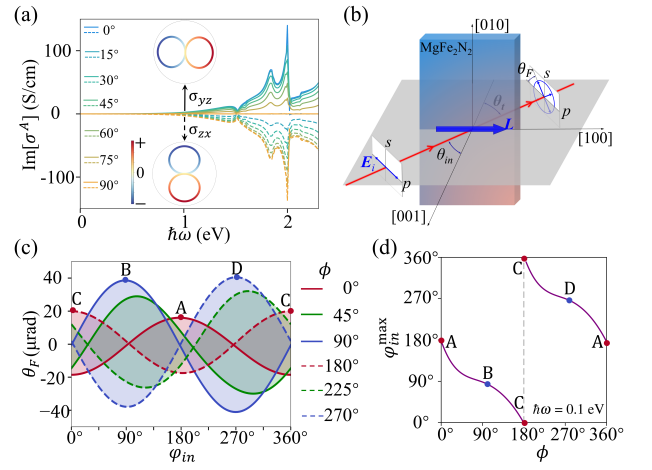


FIG. 4. Detection of Néel order (\mathbf{L}) orientation (ϕ) via magneto-optical microscopy for altermagnetic monolayer MgFe_2N_2 . (a) The imaginary parts of the antisymmetric components of σ_{yz} (solid lines) and σ_{zx} (dashed lines) of the optical conductivity as functions of photon energy ($\hbar\omega$) for different ϕ . Insets: σ_{yz} and σ_{zx} versus ϕ at fixed $\hbar\omega = 1 \text{ eV}$. (b) Schematic of the magneto-optical Faraday measurement, where a p -polarized light beam is incident on monolayer MgFe_2N_2 along the direction characterized by the polar (θ_{in}) and azimuthal (φ_{in}) angles in the spherical coordinates. θ_t and θ_F denote the refraction and the Faraday angles, respectively. φ_{in} is set to 0 in (b). (c) θ_F versus φ_{in} at fixed photon energy $\hbar\omega = 0.1 \text{ eV}$ and $\theta_{in} = 60^\circ$ for representative (\mathbf{L}) orientations, all of which exhibit 2π -periodic trigonometric dependencies. (d) The one-to-one correspondence between $\varphi_{in}^{\text{max}}$ [where maximum θ_F is achieved, as marked in (c)] and in-plane Néel order orientation ϕ with $\hbar\omega = 0.1 \text{ eV}$ and $\theta_{in} = 60^\circ$.

resulting net electric dipole can be obtained as $p_z \propto \cos(2\phi)$, which is consistent with the result from LG-based classification. As a further evidence, we have plotted the magnetic-order-induced charge density difference around Fe ions for $\phi = 0$ and $\phi = \pi/2$ in Figs. 2(d) and 2(e), respectively. Distinct charge transfer trends can be seen between the two (inverse)ferroelectric phases, serving as a direct signature of the polarization reversal.

Detection of altermagnetic Néel vector. Given the locked coupling between polarization and Néel order in altermagnetic multiferroics, precise determination of the Néel vector's crystallographic orientation becomes indispensable yet remains a significant challenge. Here, we propose to take advantage of Néel-order-dependent transport phenomena, specifically optical conductivity and resulting magneto-optical Faraday effect, to identify the Néel vector's orientation in altermagnets. Following previous analysis, we continue to employ monolayer MgFe_2N_2 as a representative material to demonstrate the proposed mechanism. First, we inspect the optical conductivity tensor, in particular the antisymmetric parts of the σ_{yz} and σ_{zx} components, for different in-plane Néel vector orientations of MgFe_2N_2 . In Fig. 4(a), we plot imaginary parts of σ_{yz} (solid lines) and σ_{zx} (dashed lines)

as a function of the photon energy for representative values of ϕ between 0 and $\pi/2$ ([100]-direction is chosen as the x -axis with $\phi = 0$). With ϕ increasing from 0 to $\pi/2$, the overall magnitude of σ_{yz} (σ_{zx}) gradually decreases (increases) from the maximum (minimum) value to the minimum (maximum) value, as clearly demonstrated by ϕ -dependent σ_{yz} and σ_{zx} for fixed photon energy of 1 eV shown in the insets. Note that σ_{yz} (σ_{zx}) vanishes at $\phi = 0$ ($\phi = \pi/2$) due to the M_x (M_y) mirror symmetry.

Building on calculations of optical conductivity tensors, we then show that in-plane Néel vector orientation could be unambiguously determined via measurements of Faraday angles. As illustrated in Fig. 4(b), we consider a p -polarized light beam incident on monolayer MgFe_2N_2 at an angle θ_{in} with respect to the z -axis and an azimuthal angle φ_{in} relative to the x -axis. Note that φ_{in} can be easily tuned between 0 and 2π by simply rotating the light beam around the z -direction. The calculated Faraday angle θ_F as a function of φ_{in} at fixed $\theta_{in} = 60^\circ$ and photon energy of 0.1 eV for representative Néel vector orientations are presented in Fig. 4(c), where θ_F exhibits a 2π -periodic trigonometric dependence on φ_{in} . We find an approximate relationship between the Néel vector orientation (ϕ) and the critical azimuthal angle (φ_{in}^{\max}) displaying the maximum θ_F value, given by $\varphi_{in}^{\max} = c_1 - \phi + c_2 \sin(2\phi)$ [c_1 and c_2 are constants with $c_1 = \pi$ ($c_1 = 3\pi$) for $\phi < \pi$ ($\phi > \pi$), see SM for details [61]], as demonstrated in Fig. 4(d) for $\theta_{in} = 60^\circ$ (see SM for other angles [61]). This one-to-one correspondence between ϕ and φ_{in}^{\max} therefore provides a feasible method to determine the Néel vector orientation and the corresponding electric polarization in altermagnetic multiferroics.

Conclusion. We have proposed a novel paradigm to achieve type-II multiferroicity through the generation of ferroelectric polarization via unconventional spin structures in altermagnets. Based on microscopic theory for electric dipole moments, we have established a direct correlation and robust locking behavior between the emergent electric polarization and altermagnetic Néel order parameter, which are further classified into eight distinct categories for 2D altermagnets described by LG symmetries. Our theory is validated by first-principles calculations on a prototypical altermagnetic multiferroic material of monolayer MgFe_2N_2 . Our work could not only facilitate studies of ME couplings in altermagnets, but also open avenues for altermagnetic spintronics.

Note Added. Recent studies have also focused on ferroelectric properties of altermagnets [49, 50, 68–71], but type-II multiferroics induced by altermagnetic order are not addressed in these works.

This work is supported by National Key Projects for Research and Development of China (Grant No. 2021YFA1400400), Natural Science Foundation of Jiangsu Province (No. BK20200007, No. BK20233001), the Natural Science Foundation of China (No. 12074181 and No. 92365203) and China Postdoctoral Science

Foundation under Grant Number 2024M761372.

* These authors contributed equally.

† hqwang@njnu.edu.cn

‡ zhanghj@njnu.edu.cn

- [1] I. I. Mazin, K. Koepf, M. D. Johannes, R. González-Hernández, and L. Šmejkal, Prediction of unconventional magnetism in doped FeSb_2 , *Proc. Natl. Acad. Sci.* **118**, e2108924118 (2021).
- [2] R. González-Hernández, L. Šmejkal, K. Vybírný, Y. Yahagi, J. Sinova, T. Jungwirth, and J. Železný, Efficient electrical spin splitter based on nonrelativistic collinear antiferromagnetism, *Phys. Rev. Lett.* **126**, 127701 (2021).
- [3] L. Šmejkal, J. Sinova, and T. Jungwirth, Beyond conventional ferromagnetism and antiferromagnetism: A phase with nonrelativistic spin and crystal rotation symmetry, *Phys. Rev. X* **12**, 031042 (2022).
- [4] I. Turek, Altermagnetism and magnetic groups with pseudoscalar electron spin, *Phys. Rev. B* **106**, 094432 (2022).
- [5] L. Šmejkal, A. H. MacDonald, J. Sinova, S. Nakatsuji, and T. Jungwirth, Anomalous hall antiferromagnets, *Nat. Rev. Mater.* **7**, 482 (2022).
- [6] J. Krempaský, L. Šmejkal, S. W. D'Souza, M. Hajaoui, G. Springholz, K. Uhlířová, F. Alarab, P. C. Constantinou, V. Strocov, D. Usanov, W. R. Pudenko, R. González-Hernández, A. Birk Hellenes, Z. Jansa, H. Reichlová, Z. Šobán, R. D. Gonzalez Betancourt, P. Wadley, J. Sinova, D. Kriegner, J. Minár, J. H. Dil, and T. Jungwirth, Altermagnetic lifting of Kramers spin degeneracy, *Nature* **626**, 517 (2024).
- [7] S. Reimers, L. Odenbreit, L. Šmejkal, V. N. Strocov, P. Constantinou, A. B. Hellenes, R. Jaeschke Ubierno, W. H. Campos, V. K. Bharadwaj, A. Chakraborty, *et al.*, Direct observation of altermagnetic band splitting in CrSb thin films, *Nat. Commun.* **15**, 2116 (2024).
- [8] R. Tamang, S. Gurung, D. Rai, S. Brahimi, and S. Lounis, Newly discovered magnetic phase: A brief review on altermagnets, [arXiv:2412.05377](https://arxiv.org/abs/2412.05377) (2024).
- [9] J. Liu, J. Zhan, T. Li, J. Liu, S. Cheng, Y. Shi, L. Deng, M. Zhang, C. Li, J. Ding, *et al.*, Absence of altermagnetic spin splitting character in rutile oxide RuO_2 , *Phys. Rev. Lett.* **133**, 176401 (2024).
- [10] J. Ding, Z. Jiang, X. Chen, Z. Tao, Z. Liu, T. Li, J. Liu, J. Sun, J. Cheng, J. Liu, *et al.*, Large band splitting in g -wave altermagnet CrSb , *Phys. Rev. Lett.* **133**, 206401 (2024).
- [11] H. Chen, Z. Wang, P. Qin, Z. Meng, X. Zhou, X. Wang, L. Liu, G. Zhao, Z. Duan, T. Zhang, *et al.*, Altermagnetic spin-splitting magnetoresistance, [arXiv:2412.18220](https://arxiv.org/abs/2412.18220) (2024).
- [12] N. Wang, J. Chen, N. Ding, H. Zhang, S. Dong, and S.-S. Wang, Magneto-optical Kerr effect and magnetoelasticity in a weakly ferromagnetic RuF_4 monolayer, *Phys. Rev. B* **106**, 064435 (2022).
- [13] X. Zhou, W. Feng, R.-W. Zhang, L. Šmejkal, J. Sinova, Y. Mokrousov, and Y. Yao, Crystal Thermal Transport in Altermagnetic RuO_2 , *Phys. Rev. Lett.* **132**, 056701 (2024).
- [14] L. Attias, A. Levchenko, and M. Khodas, Intrinsic anomalous Hall effect in altermagnets, *Phys. Rev. B* **110**,

- 094425 (2024).
- [15] P. A. McClarty and J. G. Rau, Landau Theory of Altermagnetism, *Phys. Rev. Lett.* **132**, 176702 (2024).
- [16] M. Milivojević, M. Orozović, S. Picozzi, M. Gmitra, and S. Stavičić, Interplay of Altermagnetism and Weak Ferromagnetism in Two-Dimensional RuF₄, *2D Mater.* **11**, 035025 (2024).
- [17] D. Jo, D. Go, Y. Mokrousov, P. M. Oppeneer, S.-W. Cheong, and H.-W. Lee, Weak ferromagnetism in altermagnets from alternating g -tensor anisotropy, [arXiv:2410.17386](https://arxiv.org/abs/2410.17386) (2024).
- [18] S.-W. Cheong and F.-T. Huang, Altermagnetism with non-collinear spins, *npj Quantum Mater.* **9**, 13 (2024).
- [19] L. Han, X. Fu, W. He, Y. Zhu, J. Dai, W. Yang, W. Zhu, H. Bai, C. Chen, C. Wan, *et al.*, Observation of non-volatile anomalous Nernst effect in altermagnet with collinear Néel vector, [arXiv:2403.13427](https://arxiv.org/abs/2403.13427) (2024).
- [20] S. Zeng and Y.-J. Zhao, Description of two-dimensional altermagnetism: Categorization using spin group theory, *Phys. Rev. B* **110**, 054406 (2024).
- [21] P. G. Radaelli, Tensorial approach to altermagnetism, *Phys. Rev. B* **110**, 214428 (2024).
- [22] Z. Xiao, J. Zhao, Y. Li, R. Shindou, and Z.-D. Song, Spin space groups: Full classification and applications, *Phys. Rev. X* **14**, 031037 (2024).
- [23] R.-C. Xiao, H. Li, H. Han, W. Gan, M. Yang, D.-F. Shao, S.-H. Zhang, Y. Gao, M. Tian, and J. Zhou, Anomalous-hall neel textures in altermagnetic materials, [arXiv:2411.10147](https://arxiv.org/abs/2411.10147) (2024).
- [24] Z. Qian, Y. Yang, S. Liu, and C. Wu, Fragile Unconventional Magnetism in RuO₂ by Proximity to Landau-Pomeranchuk Instability, [arXiv:2501.13616](https://arxiv.org/abs/2501.13616) (2025).
- [25] Q. Liu, X. Dai, and S. Blügel, Different facets of unconventional magnetism, *Nat. Phys.* **21**, 329 (2025).
- [26] Z. Liu and N. V. Medhekar, d -wave polarization-spin locking in two-dimensional altermagnets, [arXiv:2502.16103](https://arxiv.org/abs/2502.16103) (2025).
- [27] S.-W. Cheong and F.-T. Huang, Altermagnetism classification, *npj Quantum Mater.* **10**, 38 (2025).
- [28] S.-W. Cheong and F.-T. Huang, Kinetomagnetism and altermagnetism, [arXiv:2503.16277](https://arxiv.org/abs/2503.16277) (2025).
- [29] P. G. Radaelli and G. Gurung, Colour symmetry and non-collinear altermagnetism, [arXiv:2501.02947](https://arxiv.org/abs/2501.02947) (2025).
- [30] Z.-A. Wang, B. Li, S.-S. Zhang, W.-J. Lu, M. Tian, Y.-P. Sun, E. Y. Tsymbal, K. Wang, H. Du, and D.-F. Shao, Giant uncompensated magnon spin currents in x-type magnets, [arXiv:2502.13511](https://arxiv.org/abs/2502.13511) (2025).
- [31] Z.-F. Gao, S. Qu, B. Zeng, Y. Liu, J.-R. Wen, H. Sun, P.-J. Guo, and Z.-Y. Lu, AI-accelerated discovery of altermagnetic materials, *Nat. Sci. Rev.* **12**, nwaf066 (2025).
- [32] J.-K. Yuan, Z. Pan, and C. Wu, Unconventional magnetism in spin-orbit coupled systems, [arXiv:2504.14577](https://arxiv.org/abs/2504.14577) (2025).
- [33] Z. Zhou, X. Cheng, M. Hu, J. Liu, F. Pan, and C. Song, Crystal design of altermagnetism, [arXiv:2403.07396](https://arxiv.org/abs/2403.07396) (2024).
- [34] C.-C. Wei, E. Lawrence, A. Tran, and H. Ji, Crystal chemistry and design principles of altermagnets, *ACS Org. Inorg. Au* **4**, 604 (2024).
- [35] L. Bai, W. Feng, S. Liu, L. Šmejkal, Y. Mokrousov, and Y. Yao, Altermagnetism: Exploring New Frontiers in Magnetism and Spintronics, *Adv. Funct. Mater.* **34**, 2409327 (2024).
- [36] C. Song, H. Bai, Z. Zhou, L. Han, H. Reichlova, J. H. Dil, J. Liu, X. Chen, and F. Pan, Altermagnets as a new class of functional materials, *Nat. Rev. Mater.* [10.1038/s41578-025-00779-1](https://doi.org/10.1038/s41578-025-00779-1) (2025).
- [37] S. S. Fender, O. Gonzalez, and D. K. Bediako, Altermagnetism: A Chemical Perspective, *J. Am. Chem. Soc.* **147**, 2257 (2025).
- [38] R. Peng, J. Yang, L. Hu, W.-L. Ong, P. Ho, C. S. Lau, J. Liu, and Y. S. Ang, All-electrical layer-spintronics in altermagnetic bilayers, *Mater. Horiz.* **12**, 2197 (2025).
- [39] K. Samanta, M. Ležaić, M. Merte, F. Freimuth, S. Blügel, and Y. Mokrousov, Crystal Hall and crystal magneto-optical effect in thin films of SrRuO₃, *J. Appl. Phys.* **127**, 213904 (2020).
- [40] Y.-C. Zhang, H. Bai, D.-H. Zhang, C. Chen, L. Han, S.-X. Liang, R.-Y. Chu, J.-K. Dai, M. Sawicki, F. Pan, and C. Song, Probing the Néel Order in Altermagnetic RuO₂ Films via X-Ray Magnetic Linear Dichroism, *Chin. Phys. Lett.* **42**, 027301 (2025).
- [41] M. Raboni Ferreira, B. J. Daurer, J. Neethirajan, A. Apseros, S. Ruiz-Gómez, B. Kaulich, M. Kazemian, and C. Donnelly, Nanoscale mapping of magnetic orientations with complex x-ray magnetic linear dichroism, [arXiv:2502.08617](https://arxiv.org/abs/2502.08617), [arXiv](https://arxiv.org/abs/2502.08617) (2025).
- [42] M. Leiviskä, J. Rial, A. Bad'ura, R. L. Seeger, I. Kounta, S. Beckert, D. Kriegner, I. Joumard, E. Schmoranzeroová, J. Sinova, O. Gomonay, A. Thomas, S. T. B. Goennenwein, H. Reichlová, L. Šmejkal, L. Michez, T. Jungwirth, and V. Baltz, Anisotropy of the Anomalous Hall Effect in Thin Films of the Altermagnet Candidate Mn₅Si₃, *Phys. Rev. B* **109**, 224430 (2024).
- [43] Z. Zhou, X. Cheng, M. Hu, R. Chu, H. Bai, L. Han, J. Liu, F. Pan, and C. Song, Manipulation of the altermagnetic order in CrSb via crystal symmetry, *Nature* **638**, 645–650 (2025).
- [44] A. Wu, D. Cheng, X. Wang, M. Zeng, C. Liu, and X. Li, Optical signatures of noncentrosymmetric structural distortion in altermagnetic MnTe, [arXiv:2503.17742](https://arxiv.org/abs/2503.17742) (2025).
- [45] L. Han, X. Fu, C. Song, Y. Zhu, X. Li, Z. Zhu, H. Bai, R. Chu, J. Dai, S. Liang, *et al.*, Discovery of a large magnetic nonlinear hall effect in an altermagnet, [arXiv:2502.04920](https://arxiv.org/abs/2502.04920) (2025).
- [46] P.-J. Guo, Y. Gu, Z.-F. Gao, and Z.-Y. Lu, Altermagnetic ferroelectric LiFe₂F₆ and spin-triplet excitonic insulator phase, [arXiv:2312.13911](https://arxiv.org/abs/2312.13911) (2023).
- [47] J. Matsuda, H. Watanabe, and R. Arita, Multiferroic collinear antiferromagnet with hidden altermagnetic split, [arXiv:2412.20128](https://arxiv.org/abs/2412.20128) (2024).
- [48] Y. Sheng, J. Liu, J. Zhang, and M. Wu, Ubiquitous van der waals altermagnetism with sliding/moire ferroelectricity, [arXiv:2411.17493](https://arxiv.org/abs/2411.17493) (2024).
- [49] M. Gu, Y. Liu, H. Zhu, K. Yananose, X. Chen, Y. Hu, A. Stroppa, and Q. Liu, Ferroelectric Switchable Altermagnetism, *Phys. Rev. Lett.* **134**, 106802 (2025).
- [50] X. Duan, J. Zhang, Z. Zhu, Y. Liu, Z. Zhang, I. Žutić, and T. Zhou, Antiferroelectric Altermagnets: Antiferroelectricity Alters Magnets, *Phys. Rev. Lett.* **134**, 106801 (2025).
- [51] L. Camerano, A. O. Fumega, J. L. Lado, A. Stroppa, and G. Profeta, Multiferroic nematic d-wave altermagnetism driven by orbital-order on the honeycomb lattice, [arXiv:2503.19987](https://arxiv.org/abs/2503.19987) (2025).
- [52] S. Wang, W.-W. Wang, J. Fan, X. Zhou, X.-P. Li, and L. Wang, Two-dimensional dual-switchable ferroelectric altermagnets: Altering electrons and magnons, [arXiv:2504.19585](https://arxiv.org/abs/2504.19585) (2025).
- [53] S. Dong, H. Xiang, and E. Dagotto, Magnetoelectricity

- in multiferroics: A theoretical perspective, *Nat. Sci. Rev.* **6**, 629 (2019).
- [54] C. Liu, W. Ren, and S. Picozzi, Spin-chirality-driven multiferroicity in van der waals monolayers, *Phys. Rev. Lett.* **132**, 086802 (2024).
- [55] S. Stavrić, G. Cuono, B. Yang, Á. R. Puente-Uriona, J. Ibañez-Azpiroz, P. Barone, A. Droghetti, and S. Picozzi, Giant non-reciprocal band structure effect in a multiferroic material, [arXiv:2503.01534](https://arxiv.org/abs/2503.01534) (2025).
- [56] H. Murakawa, Y. Onose, S. Miyahara, N. Furukawa, and Y. Tokura, Ferroelectricity induced by spin-dependent metal-ligand hybridization in $\text{Ba}_2\text{CoGe}_2\text{O}_7$, *Phys. Rev. Lett.* **105**, 137202 (2010).
- [57] J. Zhang, Y. Zhou, F. Wang, X. Shen, J. Wang, and X. Lu, Coexistence and coupling of spin-induced ferroelectricity and ferromagnetism in perovskites, *Phys. Rev. Lett.* **129**, 117603 (2022).
- [58] Y. Zhou, H. Ye, J. Zhang, and S. Dong, Double-leaf Riemann surface topological converse magnetoelectricity, *Phys. Rev. B* **110**, 054424 (2024).
- [59] C. Jia, S. Onoda, N. Nagaosa, and J. H. Han, Bond electronic polarization induced by spin, *Phys. Rev. B* **74**, 224444 (2006).
- [60] M. Matsumoto, K. Chimata, and M. Koga, Symmetry analysis of spin-dependent electric dipole and its application to magnetoelectric effects, *J. Phys. Soc. Jpn.* **86**, 034704 (2017).
- [61] See the Supplemental Material for additional information about the methods and additional data and discussion.
- [62] Y. Wu, Z. Zeng, H. Lu, X. Han, C. Yang, N. Liu, X. Zhao, L. Qiao, W. Ji, R. Che, *et al.*, Coexistence of ferroelectricity and antiferroelectricity in 2d van der waals multiferroic, *Nat. Commun.* **15**, 8616 (2024).
- [63] F. Matsukura, Y. Tokura, and H. Ohno, Control of magnetism by electric fields, *Nat. Nanotechnol.* **10**, 209 (2015).
- [64] S. Jiang, L. Li, Z. Wang, K. F. Mak, and J. Shan, Controlling Magnetism in 2D CrI_3 by Electrostatic Doping, *Nat. Nanotechnol.* **13**, 549 (2018).
- [65] Q. Song, C. A. Occhialini, E. Ergeçen, B. Ilyas, D. Amoroso, P. Barone, J. Kapteghian, K. Watanabe, T. Taniguchi, A. S. Botana, S. Picozzi, N. Gedik, and R. Comin, Evidence for a single-layer van der Waals multiferroic, *Nature* **602**, 601 (2022).
- [66] H. Murakawa, Y. Onose, S. Miyahara, N. Furukawa, and Y. Tokura, Comprehensive study of the ferroelectricity induced by the spin-dependent d - p hybridization mechanism in $\text{Ba}_2X\text{Ge}_2\text{O}_7$ ($X = \text{Mn}, \text{Co}, \text{and Cu}$), *Phys. Rev. B* **85**, 174106 (2012).
- [67] C. Jia, S. Onoda, N. Nagaosa, and J. H. Han, Microscopic theory of spin-polarization coupling in multiferroic transition metal oxides, *Phys. Rev. B* **76**, 144424 (2007).
- [68] W. Sun, C. Yang, W. Wang, Y. Liu, X. Wang, S. Huang, and Z. Cheng, Proposing Altermagnetic-Ferroelectric Type-III Multiferroics with Robust Magnetoelectric Coupling, *Adv. Mater.* , 2502575 (2025).
- [69] L. Šmejkal, Altermagnetic multiferroics and altermagnetoelectric effect, [arXiv:2411.19928](https://arxiv.org/abs/2411.19928) (2024).
- [70] Z. Zhu, X. Duan, J. Zhang, B. Hao, I. Zutic, and T. Zhou, Two-dimensional ferroelectric altermagnets: From model to material realization, [arXiv:2504.06258](https://arxiv.org/abs/2504.06258) (2025).
- [71] Y. Zhu, M. Gu, Y. Liu, X. Chen, Y. Li, S. Du, and Q. Liu, Sliding ferroelectric control of unconventional magnetism in stacked bilayers, [arXiv:2502.17095](https://arxiv.org/abs/2502.17095) (2025).